Article

Journal of the Brazilian Chemical Society

https://dx.doi.org/10.21577/0103-5053.20240095

J. Braz. Chem. Soc. **2024**, *35*, 11, e-20240095, 1-14

U-PEO:CuZnAl as a Recyclable Bifunctional Composite for Absorption/Degradation of Azo-Dyes

Gustavo Palácio,[a] *Camila T. Piza,*[a] *Maria L. Batista,*[a] *Caio C. dos Santos,*[a] *Sandra H. Pulcinelli*[a] *and Celso V. Santilli*[*,a]

[a]*Instituto de Química da Universidade Estadual Paulista "Júlio de Mesquita Filho" (UNESP), 14800-060 Araraquara-SP, Brazil*

The catalytic activity of layered double hydroxide (LDH) and the aqueous solution absorption capacity of ureasil polyethylene oxide (U-PEO) were combined to produce an easily recyclable solid-liquid (S-L) reactor (U-PEO:LDH). Scanning electron microscopy (SEM), X-ray diffraction (XRD) and small-angle X-ray scattering (SAXS) of LDH (CuZnAl), U-PEO, and U-PEO:LDH confirmed the layered structure of the catalyst and evidenced its inclusion in the free volume of U-PEO matrix. The catalytic activity of the CuZnAl in the composite prepared with different amounts of LDH, towards degradation of the Acid Blue 29 (AB29) dye by a heterogeneous Fenton-like process was investigated, and the results evidenced a maximum efficiency (96%) for composite with 10 wt.% of LDH. Recyclability assessments demonstrated that the superior performance of the U-PEO:LDH reactor was sustained over several cycles (4). The U-PEO:LDH reactor proposed in this work has excellent potential as a heterogeneous catalyst for effective dye removal in environmental applications.

Keywords: hybrid materials, LDH, Fenton-like reactions, heterogeneous catalyst

Introduction

The development of alternative routes and materials to effectively restore the water quality would be of great value since a variety of pollutants are emerging from current inadequate water treatment methods like adsorption, coagulation, and ultrafiltration.[1,2] Moreover, these classical methods mainly transfer the contaminant from wastewater to solid wastes.[3] In this respect, technologies based on advanced oxidative processes (AOPs) can provide efficient removal from wastewater of organic pollutants with high chemical stability and/or low biodegradability.[4,5] AOPs are especially attractive due to the ability to oxidize a wide range of organic contaminants, at near-ambient temperature and pressure,[6] enabling the complete decomposition of organic pollutants into nontoxic products, with the overall processes leading to the mineralization of contaminants to CO_2, H_2O, and inorganic salts.[7]

Among the AOPs, the Fenton process employing a heterogeneous catalyst is one of the most cost-effective.[8] The classical Fenton reaction involves the reduction of H_2O_2 with Fe^{2+}, generating highly reactive hydroxyl radicals ($HO^{\bullet}$) that can non-selectively degrade most organic contaminants, due to their high redox potential (E_0 ($HO^{\bullet}$/H_2O) = 2.8 V).[6,9] As an alternative to Fe^{2+}, other transition metals such as Cu^{2+} and Mn^{2+} can also promote the generation of hydroxyl radicals,[10,11] with copper showing very similar redox properties as iron, in terms of its reactivity towards H_2O_2. Compared to Fe, Cu facilitates the interfacial electron transfer, accelerating the regeneration of the catalyst.[12] Moreover, copper has good pH adaptability, which is proved to be a significant advantage for the replacement of iron in the Fenton reaction.[13] Both the monovalent (Cu^{+}) and divalent (Cu^{2+}) oxidation states of copper react easily with H_2O_2 (equations 1 and 2), analogous to the Fe^{2+}/H_2O_2 and Fe^{3+}/H_2O_2 systems (equations 3 and 4), k being the rate constant.[14-16]

$$Cu^{2+} + H_2O_2 \rightarrow Cu^{+} + HO_2^{\bullet} + OH^{-} \quad (k = 4.6 \times 10^2\ M^{-1}\ s^{-1}) \quad (1)$$

$$Cu^{+} + H_2O_2 \rightarrow Cu^{2+} + HO^{\bullet} + HO^{-} \quad (k = 1.0 \times 10^4\ M^{-1}\ s^{-1}) \quad (2)$$

$$Fe^{2+} + H_2O_2 \rightarrow Fe^{3+} + HO^{\bullet} + OH^{-} \quad (k = 63 - 76\ M^{-1}\ s^{-1}) \quad (3)$$

$$Fe^{3+} + H_2O_2 \rightarrow Fe^{2+} + HO_2^{\bullet} + H^{+} \quad (k = 0.001 - 0.01\ M^{-1}\ s^{-1}) \quad (4)$$

*e-mail: cv.santilli@unesp.br
Editor handled this article: Ítalo O. Mazali (Guest)
The first lecture by Prof Luiz Osvaldo Alves I attended at the IQ/UNESP started with a photo of a bakery, in which it was announced: Our bread has neither chemistry nor composition!

However, there is a considerable difference in the aqueous solubility characteristics of Cu^{2+} and Fe^{3+}. The iron aquo complex $[Fe(H_2O)_6]^{3+}$ is insoluble at pH > 5, while the corresponding copper complex $[Cu(H_2O)_6]^{2+}$ is predominant under neutral pH conditions.[17] This means that the Cu^{2+}/H_2O_2 Fenton-like system works over a broader pH range, compared to the Fe^{3+}/H_2O_2 redox system that only acts under acidic conditions, with the associated high costs of chemicals required to acidify effluents and the risk of serious corrosion of equipment.

Several heterogeneous catalysts for Cu/Fenton-like reactions have been reported, including modified aluminates,[18,19] zirconia,[20] CuO and TiC nanoparticles,[21] Cu-ligand complexes,[22-24] and Cu-hydroxide nitrates.[25] Other promising catalysts belong to the layered double hydroxide (LDH) family, also known as hydrotalcite-like compounds or anionic clays.[26] The general formula of LDH is $[M^{2+}_{(1-x)}M^{3+}_{x}(OH)_2]_{layer}[A^{n-}_{x/n}y_zH_2O]_{interlayer}$, where M^{2+} and M^{3+} are divalent and trivalent metal cations, respectively, occupying the octahedral interstices of layers, while A^{n-} represents organic or inorganic anions intercalated in the galleries of the lamellar structure.[27] LDHs are widely used as heterogeneous catalysts, due to their tunable chemical composition, high redox activity, environmental friendliness, ion exchange capacity, high specific surface area, memory effect, nontoxicity, and low cost.[28-33] Their unique anisotropic structures mean that LDHs are among the few layered materials with a positive structural charge that enables the adsorption of negatively charged substances.[32-34] Alves and co-workers[34,35] highlighted the key roles of the very high number of exchangeable anions (2-5 mmol g^{-1}) and the high surface areas (10-120 m^2 g^{-1}) of LDHs in their functional performance as ion exchangers/adsorbents for the removal from contaminated waters of toxic anions such as borates, dichromates, selenates, fluorides, phenols, dyes, pesticides, and phosphates, among others. However, depending on the ionic strength, pH, and nature of the ionic species, delamination of the lamellar structure can occur, hindering the recovery and reuse of powdered LDH in cyclic wastewater treatments.[35] Table 1 summarizes the characteristics of some LDH catalysts used in Fenton and Fenton-like degradation of different pollutants in water solution. A more extensive list of different LDHs applied in Fenton and Fenton-like systems for efficient pollutants removal was recently reviewed by Pelalak *et al*.[36]

Although the excellent progress in heterogeneous catalysis, in majority of those studies presented in Table 1, the catalyst was employed as a powder dispersed in the wastewater solution containing its respective target molecule. In order to avoid some structural aggregation-delamination issues, LDHs were loaded with other substances, such as carbon-based materials, to form stable and efficient Fenton-like catalysts, as shown by the combination of CuMgAl-LDH with reduced graphene

Table 1. LDH based materials used as Fenton-like catalysts for environmental remediation

Catalyst	Pollutant concentration	Experimental conditions	Removal efficiency	Reference
CuNiFeLa-LDH La:(Fe + La) = 0.1	florfenicol 10 mg L^{-1}	5 mmol L^{-1} of H_2O_2 and 0.25 g L^{-1} of catalyst in 50 mL of florfenicol solution at neutral pH	95% after 180 min	13
MgFe-LDH Mg:Fe = 3 MnMgFe-LDH	methylene blue 20 mg L^{-1}	H_2O_2 (20 wt.%) and 0.03 g of catalyst in 10 mL of water	80% for MnMgFe and 75% for MgFe after 5 cycles	26
$Cu_1Ni_2Sn_{0.75}$ LDH	phenol 100 mg L^{-1}	H_2O_2 (30 wt.%) and 0.1 g of catalyst in 100 mL phenol solution, T = 50 °C	97%	37
CuAl-LDH/carbon fiber composites Cu:Al = 2	ammonia nitrogen 25 mg L^{-1}	visible light irradiation, H_2O_2 and catalyst dosage variable, optimum pH = 8	95% for CuAl-LDH and 98% for CuAl/CF-LDH, 80% after 10 cycles	38
Cu_xNi_yCo-LDH ((Cu+Ni):Co = 3) nanosheets supported GO	tetracycline 20 mg L^{-1}	10 mmol L^{-1} of H_2O_2 and 60 mg L^{-1} of catalyst at pH = 10.2	96% in 40 min and 80% after 5 cycles	39
CuMgFe-LDH (Mg:Fe = 3)	sulfathiazole 150 μg L^{-1}	H_2O_2: 0, 2, 4, and 6 mmol L^{-1} and catalyst: 0.2-1.0 g L^{-1} at pH = 7.5	100% in 90 min	40

LDH: layered double hydroxide; GO: graphene oxide.

oxide (GO), which exhibited a tri-phasic synergistic effect with enhanced catalytic performance.[41] This kind of methodology was utilized by Peng *et al*.[38] to prepare CuAl-LDH for the degradation of ammonia nitrogen. The authors have found that CuAl-LDH aggregated easily, while the addition of carbon fiber (CF) prevented the aggregation of the delaminated LDH nanosheets. Despite the eco-friendly LDH-structure properties, the traditional heterogenous Fenton-like process includes secondary wastewater contaminations caused by the catalyst dispersion, imposing some necessary additional procedures to recover it from the solution.

In order to solve this problem, the present work proposes the use of an insoluble and hydrophilic organic-inorganic hybrid (OIH) material as host matrix for immobilization of the LDH catalyst, resulting in a new U-PEO:CuZnAl (OIH:LDH) solid-liquid (S-L) reactor. The OIH host material employed was a siloxane-polyether (U-PEO) based on poly(ethylene oxide) (PEO) with molecular weight of 1900 g mol^{-1}, where the organic and inorganic moieties are linked by ureasil bridges.[42] This OIH is suitable for this type of application due to its attractive characteristics, provided by the synergic contributions of the organic and inorganic moieties. These include rigidity and insolubility of the siloxane crosslinking nodes,[43] dimensional stability and hydrogel (swelling) behavior resulting from the hydrophilicity and flexibility of PEO,[44] and the presence of two different polar sites in the PEO chains, namely carbonyl-like and ether-like oxygens,[45,46] enabling the occurrence of guest-host (OIH-LDH) interactions.[44] The easy and versatility of the sol-gel processing of this U-PEO were exploited in the preparation of blends with hydrophobic poly(propylene oxide) (PPO), nanocomposites with natural montmorillonite clay, and superparamagnetic $CoFe_2O_4$ nanoparticles in order to control the water swelling,[47] the drug releasing rate[48] and the localized drug delivery induced by magnetic hyperthermia,[49] respectively.

Therefore, the aim of this work was to investigate the structural and catalytic properties of the new OIH:LDH, based on U-PEO:CuZnAl, as a bifunctional material suitable for the absorption/degradation of industrial azo dyes, with the additional advantages of easy recovery from wastewater and potential for reuse. The selection of this LDH formulation was based on the Cu Fenton-like catalytic activity and the absence of activity of Zn and Al which guarantees the stability of the LDH layers during the cupper redox reactions (equations 1 and 2). To validate the concept, Acid Blue 29 (AB29) was chosen as a target molecule for degradation according to the Fenton mechanism.[6]

Experimental

Synthesis

The CuZnAl LDH was prepared at ca. 25 °C by the coprecipitation method, using a well-known procedure.[50] An aqueous solution (0.35 mL) containing 18.36 mmol of $Cu(NO_3)_2.3H_2O$ (Sigma-Aldrich, CAS No. 10031-43-3, Merck, São Paulo, Brazil), 73.44 mmol of $Zn(NO_3)_2.6H_2O$ (Sigma-Aldrich, CAS No. 10196-18-6, Merck, São Paulo, Brazil), and 30.60 mmol of $Al(NO_3)_3.9H_2O$ (Sigma-Aldrich, CAS No. 7784-27-2, Merck, São Paulo, Brazil) was added dropwise to 1.60 L of an aqueous solution of 91.80 mmol Na_2CO_3 (Sigma-Aldrich, CAS No. 497-19-8, Merck, São Paulo, Brazil), under vigorous stirring. The mixture was maintained at pH 8 by adding aqueous 2 mol L^{-1} NaOH (Sigma-Aldrich, ≥ 97% purity, CAS No. 1310-73-2, Merck, São Paulo, Brazil) during the precipitation. The (Cu and Zn):Al (M^{2+}:M^{3+}) atomic ratio in the starting solution was adjusted to 3:1, while the Cu:Zn atomic ratio was 1:4. The precipitate was then isolated by filtration, washed thoroughly with deionized water several times, and dried at ambient temperature, under reduced pressure, in the presence of silica gel. This methodology enabled the preparation of CuZnAl LDH containing 15 wt.% of copper.

The ureasil-PEO hybrid precursor used to prepare the host OIH was synthesized according to a well-known sol-gel route, using commercially available reagents.[51] Briefly, the ureasil (U) crosslinking agent 3-(isocyanatopropyl) triethoxysilane (IsoTrEOS, Sigma-Aldrich, 95% purity, CAS No. 24801-88-5, Merck, São Paulo, Brazil) was covalently bonded to terminal aminopropyl groups of the end-functionalized PEO (Jeffamine ED-2003, CAS No. 65605-36-9, Merck, São Paulo, Brazil), leading to formation of the urea group (–HNC(=O)NH–)[52] and, consequently, the ureasil grouping (urea-siloxane). Typically, 4 g of IsoTrEOS and 16 g of Jeffamine ED-2003 were stirred together in ethanolic solution, at an OIH:ethanol mass/volume ratio of 1:2, under reflux for 6 h at 78 °C. The ethanolic solution containing the OIH precursor $(EtO)_3Si–(CH_2)_3NHC(=O)NHCH(CH_3)CH_2–$(polyether)$–OCH_2CH(CH_3)NHC(=O)NH(CH_2)_3–Si(OEt)_3$ was used in the preparation of the LDH-OIH composite.

The LDH-OIH conjugation was performed by the dispersion of CuZnAl in the OIH precursor solution maintained under sonication at 30 kHz (VC 501 sonicator, Vibracel, São Paulo, Brazil) for 5 min. In the next step, the acid-catalyzed sol-gel reactions involving the $Si(OEt)_3$ were promoted by the addition of 40 μL of 10^{-2} mol L^{-1} HCl (Sigma-Aldrich, CAS No. 7647-01-0, Merck, São Paulo, Brazil) to 1.6 mL of the ethanolic solution containing the

hybrid precursor (equivalent to 0.5 g of the solid hybrid precursor). This procedure resulted in the formation of a crosslinked PEO network with two main polar oxygen sites, the ether-type oxygen and the carbonyl-type oxygen. Solid xerogels were obtained after drying for 12 h at ambient temperature, under vacuum. The amounts of LDH (x) used to prepare these composite materials, hereafter called U-PEO:xCuZnAl, were varied to obtain mass percentages of 7, 10, 20, and 30%, relative to the OIH mass (0.5 g). This conjugation strategy, represented in Scheme 1, was based on the affinity of the positive charge of the LDH layer, resulting from the divalent and trivalent metal cations occupying the octahedral interstices of the layers, for the different polar oxygen sites of the U-PEO matrix.[53]

Characterization

The morphology of particles present in dried LDH powder and OIH:xLDH S-L reactor was analyzed by scanning electron microscopy (SEM) performed with a JSM-IT500HR microscope (JEOL, Japan) equipped with secondary (SE) and back-scattered electrons (BSE) detectors, used for topological and chemical images, respectively.

The specific area of the dried LDH powder was determined by N_2 adsorption-desorption isotherms acquired at 77 K using a Micromeritics ASAP 2010 instrument (Norcross, GA, USA). The Brunauer-Emmett-Teller (BET) equation was used to calculate the specific area.[54]

The hydrodynamic diameter and the zeta potential (ζ-potential) of the LDH powder dispersion were obtained by dynamic light scattering (DLS) and electrophoretic mobility measurements using a Zetasizer analyzer (Malvern Panalytical, CB, UK). The dispersion was prepared by the addition of 4 mg of LDH to 15 mL of sodium nitrate electrolyte solution (1 mmol L^{-1}), followed by 10 min of ultrasonication. An auto-titration set-up was used to adjust the pH of the suspension by injecting a dilute aqueous solution of HNO_3 (0.5 mol L^{-1}) or NaOH (0.1 mol L^{-1}).

The crystalline phases were identified by powder X-ray diffraction (XRD) measurements performed with a Siemens D5000 diffractometer (Siemens, Karls-ruhe, Germany) operated with Cu Kα radiation (λ = 1.5405 Å) monochromatized by a curved graphite single crystal, 6.0 mm detector slits, and 2θ from 2 to 70°, with a 0.02 step every 3 s.

The nanostructures of the OIH host matrix, LDH powder, and OIH:xLDH S-L reactor samples were analyzed by small-angle X-ray scattering (SAXS) measurements performed at the SAXS1 beamline of the Laboratório Nacional de Luz Síncroton (LNLS, Campinas, Brazil). The beamline was equipped with a 2D Pilatus 300 K detector located 910.9 mm from the sample, recording the image of the scattering intensity, I(**q**), as a function of the modulus of the scattering vector, $\mathbf{q} = 4\pi/\lambda\sin(\varepsilon/2)$, where λ is the X-ray wavelength and ε is the X-ray scattering angle. The data were normalized considering the varying intensity of the direct X-ray beam, the detector sensitivity, and the sample transmission. The intensity of the parasitic scattering due to the cell windows and vacuum was subtracted from the total scattering intensity.

The crystalline fraction of the polymer was determined from differential scanning calorimetry (DSC) measurements performed with a Q100 analyzer (TA Instruments, New Castle, DE, USA). The samples were heated at 5 °C min^{-1} from −90 to 100 °C, with nitrogen as the purge gas at a flow rate of 50 mL min^{-1}. The melting enthalpy (ΔH_m) was recorded during the first heating run. The degree of crystallinity (D_C) was calculated from the relationship between ΔH_m and the standard melting enthalpy for 100% crystalline PEO (ΔH_p = 196.4 J g^{-1}), according to the following equation:[44]

$$D_C\,(\%) = (\Delta H_m/\Delta H_p) \times 100 \quad (5)$$

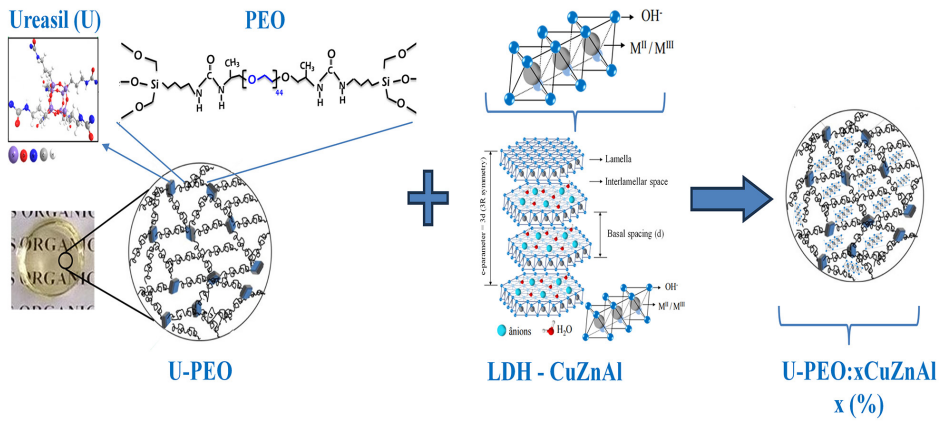

Scheme 1. Schematic representation of the conjugation of OIH (left) and LDH (center) to form the U-PEO:xCuZnAl composite (right).

Fourier transform infrared spectroscopy (FTIR) measurements were performed using a Bruker VERTEX 70 instrument (Bruker, Germany) operated in attenuated total reflection mode (ATR-FTIR). Spectra were acquired in the range from 4000 to 400 cm^{-1}, with resolution of 4 cm^{-1} and 64 scans.

Degradation experiments

The catalytic activity of the prepared OIH:xLDH S-L reactor was evaluated during experiments performed in the dark with 3 mL of 15 mg L^{-1} Acid Blue 29 (AB29, molecular formula: $C_{22}H_{14}N_6Na_2O_9S_2$, molecular weight: 616.49 g mol^{-1}, CAS No. 5850-35-1) solution, at neutral pH (ca. 7.3) and ambient temperature, under magnetic stirring (1200-1400 rpm). The conditions that will be mentioned hereafter as standard conditions (SC), were a dye solution containing 0.1 mg L^{-1} of OIH:xLDH catalyst and 0.005 mol L^{-1} of H_2O_2. Dye degradation by the Fenton-like reaction was monitored using the AB29 absorption band (λ_{max} = 602 nm), employing a Cary 60 UV-Vis spectrophotometer (Agilent Technologies, Santa Clara, CA, USA). The UV-Vis absorption spectra were recorded in the spectral range from 200 to 800 nm during the absorption/degradation reaction. The AB29 decolorization (%) was calculated as follows:[55,56]

$$\text{Efficiency}(\%) = \left(\frac{A_0 - A_t}{A_0} \right) \times 100 \quad (6)$$

where, A_0 is the initial absorption of the dye, and A_t is the absorption at time t.

The reuse capacity of the OIH:xLDH S-L reactor was evaluated using four cycles of 120 min. The S-L reactor was removed from the degradation solution and dried at ambient temperature, under vacuum, for evaporation of water. The recovered S-L reactor was then added to a fresh 15 mg L^{-1} AB29 solution to run the subsequent experiment.

Results and Discussion

Morphological and structural features

The morphological features of the LDH, OIH and OIH:xLDH materials were investigated from the SEM analysis detailed in Figure 1. As expected, the SE images of the LDH powder (Figures 1a and 1b) evidenced the platelet-like morphology of particles. The observed face-edge aggregation is a manifestation of the electrostatic interaction between negative charge density of the layer edge and the positive charge of the layer surface. This process results in hierarchical spheroidal aggregates with average size of 2.6 ± 0.9 μm. Any remarkable topological contrast was observed in the image of the OIH (Figure 1c), confirming the homogenous structure of the network formed from ureasil cross-linked PEO chains (U-PEO). The BSE images of OIH:xLDH composite evidenced that the interaction between the polar ether type oxygen of PEO chain with the positive charges surface of LDH platelet hamper the edge-surface aggregation, favoring the twisted branching of platelets. Throughout the elongate morphology, the formation of cross platelets-like occurs, which gives rise to the growth of primary and secondary branches. The comparison of these BSE images (Figures 1d-1e) evidences the increasing quantity of the hierarchical branched morphology with the percentage of LDH present in the OIH:xLDH composite.

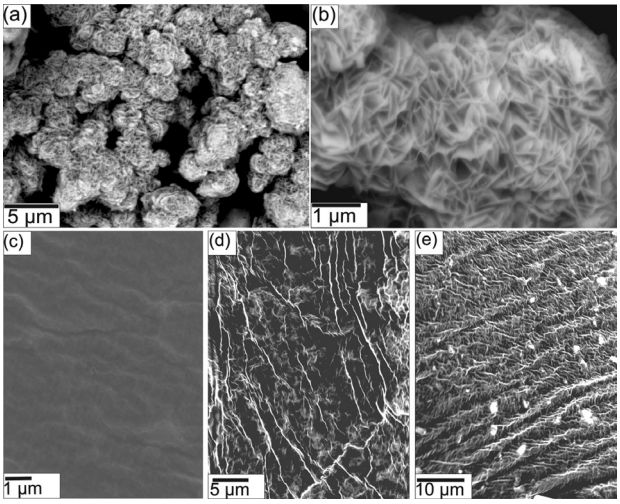

Figure 1. SEM images of CuZnAl powder (a) and (b), U-PEO matrix (c) and U-PEO:10CuZnAl (d), and U-PEO:30CuZnAl (e) OIH:xLDH composites.

The specific surface area and plate-like morphology of LDH particles was availed from the nitrogen adsorption-desorption isotherms displayed in Figure S1 (Supplementary Information (SI) section). The continuous increase of $N_{2(g)}$ volume at relative pressure near to 1 is characteristic of type II isotherms of solids with pores size larger than 50 nm (macropores).[54] Moreover, there is no evidence of hysteresis loop between the adsorption and desorption branches, indicating the absence of capillary condensation, a characteristic feature of the plate-like texture of pores wall formed by un-pillarized platelets.[54] Furthermore, the BET specific surface area equal to 72 m^2 g^{-1} is consistent with values previously reported for CuZnAl.[57] Therefore, the results from nitrogen adsorption demonstrated that the LDH powder surface properties are suitable for catalytic applications, considering the availability of adsorption sites provided by its relatively high surface value.

As expect from the structural positive charge of LDH lamellas, the colloidal dispersion exhibited high positive zeta potential (30-36 mV) in a broad range of pH (3-8) as displayed in Figure 2. The near invariance of ζ-potential in this pH range indicates the increasing acidity does not cause significant protonation of the LDH platelet surface (equation 7). The decreasing of ζ-potential values observed when the pH increases from 8 to 10 can be caused by hydroxyl deprotonation of the CuZnAl-LDH particles according to equation 8.

$$M–OH + H^+ \Leftrightarrow M–OH_2^+ \quad (7)$$

$$M–OH + OH^- \Leftrightarrow M–O^- + H_2O \ (M = Cu, Zn \text{ or } Al) \quad (8)$$

This decrease in the zeta potential value was not enough to drops to zero and achieve the isoelectric point, which occurs near pH 11.[58,59] As a consequence of the high colloidal stability achieved by high ζ-potential, a single hydrodynamic size distribution, with maximum near to 140 nm (Figure 2b), was observed for pH between 3 and 8. The decrease of ζ-potential favors the aggregation and the growth of multimodal size distribution similar to that observed in Figure 2c, for sample at pH 9.7. Therefore, these results demonstrated the near invariance of LDH surface proprieties indicating that the contribution of protonation and deprotonation (equation 3) can be neglected working in a pH range of 3-8. This feature gives strong versatility to the employment of CuZnAlLDH as catalyst for dyes degradation of a broad diversity of wastewater solutions.

Figure 3 shows the X-ray diffractograms for the OIH host (U-PEO), the LDH powder (CuZnAl), and the OIH:xLDH S-L reactor (U-PEO:xCuZnAl). The diffractogram for the U-PEO (x = 0) displayed a broad peak centered at around 21°, attributed to the amorphous siloxane phase.[60] This broad peak was also present in the OIH:xLDH diffractogram, together with diffraction peaks characteristic of the periodic layered arrangement of the LDH, similar to the diffraction pattern characteristic of the hydrotalcite isomorph (ICDD pattern 01-089-0460). The basal distance (d_{00l}) calculated from the Bragg equation ($n\lambda = 2d\sin\theta$), using the (003) and (006) diffraction peaks, was 7.56 ± 0.3 Å for the CuZnAl LDH and the U-PEO:CuZnAl S-L reactor, coinciding with the value observed for carbonate intercalation in LDH.[60] The invariance of the d_{00l} with the amount of CuZnAl revealed that the LDH structural organization was preserved after conjugation with U-PEO.

The nanostructural features of the OIH, the LDH, and the OIH:xLDH S-L reactor were revealed from the SAXS log-log curves shown in Figure 4a. The U-PEO OIH exhibited a single broad peak at around $\mathbf{q}_{max}$ = 1.9 nm^{-1}, ascribed to spatial correlation between the regularly spaced siloxane crosslink nodes.[51] The basal reflection corresponding to the LDH interlayer distance was not apparent in the SAXS curves, since the (003) peak occurs at **q** of ca. 10 nm^{-1}, which was outside the range of the experimental data.[61] The LDH SAXS curves displayed a linear behavior characteristic of power law decay of the scattering intensity ($I(\mathbf{q}) \propto \mathbf{q}^{-\alpha}$), described by Porod,[62] where the exponent α gives information about the shape of the particles and the state of agglomeration.[48] The slopes of these linear regions corresponded to α = 3.4, a value lower than the classical Porod behavior (α = 4) expected for a two-electron density system with sharp and smooth interfaces. The observed α value indicated that the LDH did not satisfy the two-electron density model, probably due to the inhomogeneity of the electron density of the

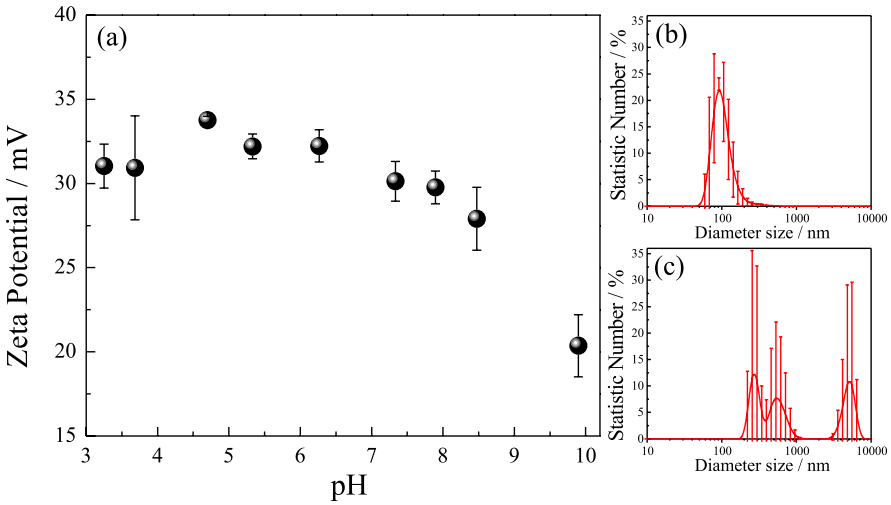

Figure 2. Dependence of ζ-potential with the pH for aqueous suspension of CuZnAl (a); hydrodynamic size distribution of CuZnAl powder in aqueous suspension at pH 4 (b) and 9.7 (c).

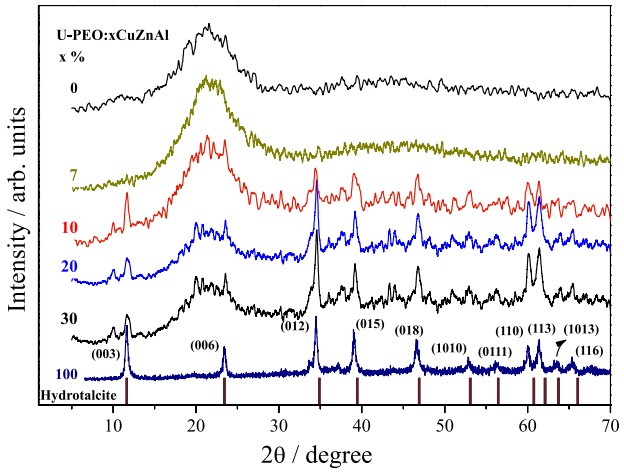

Figure 3. X-ray diffractograms at ambient temperature for the U-PEO (x = 0%) host matrix, the U-PEO:xCuZnAl S-L reactor with different percentages (x) of LDH, and the CuZnAl powder (x = 100%).

stratified structure formed by the CuZnAl layer and the interlayer gallery.[63] After the OIH:xLDH integration, the SAXS curve for the S-L reactor showed a combination of the two individual behaviors, with the LDH power law contribution in the range $\mathbf{q} < 1$ nm^{-1} ($\alpha_{LDH} = \alpha_{U\text{-}PEO:LDH} = 3.4$) and a correlation peak, less intense than that of U-PEO, in the range $\mathbf{q} > 1$ nm^{-1}. The latter feature characterized the decrease of the electron density contrast between the siloxane nodes and the PEO chains, due to the dispersion of the LDH particles in the U-PEO matrix.

In order to obtain the best evidence of the correlation peak, the contribution of the power law decay was subtracted from U-PEO:xLDH experimental curve. Considering the superposition of curves corresponding to the sample with different x%, for clarity only the subtracted curve for U-PEO:xLDH with x = 10% was displayed in Figure 4b. The maximum position ($\mathbf{q}_{max} = 1.3$ nm^{-1}) of the resulting correlation peak was lower than observed for the U-PEO matrix ($\mathbf{q}_{max} = 1.9$ nm^{-1}). This downshift reflected the increase of the average correlation distance ($D = 2\pi/\mathbf{q}_{max}$)[42] between the siloxane nodes from 3.3 nm for U-PEO to 4.8 nm for U-PEO:10CuZnAl. This finding confirmed that LDH occupied the free volume between the polyether chains of the host U-PEO (Scheme 1), causing reorganization of the segmental conformation of the PEO chains. A plausible explanation was the conversion from a helical-like conformation[64] to a stretched-like conformation, with consequent increase of the amorphous fraction.

Thermal properties and local coordination

The effect of LDH conjugation on the crystallinity of the U-PEO matrix was evaluated using DSC (Figure 5) and FTIR (Figure 6) analyses. The DSC curve for the pure U-PEO elastomer was composed of two events: (*i*) change of the heat flux capacity (ΔCp) at –43 ºC, characteristic of second order (glass ↔ rubber) transitions, ascribed to the glass transition (T_g);[45] and (*ii*) an endothermic peak, with minimum at around 28 °C, characteristic of first order (crystallization ↔ melting) transition, ascribed to the melting of host U-PEO crystalline domains.[44] The experimental value of the glass transition temperature (T_g), the melting temperature (T_m), the melting enthalpy (ΔH_m) and the percentage of crystalline PEO phase (D_c) are displayed in Table 2. It is important to note that T_g and T_m values decrease continuously by increasing the percentage (x%) of LDH present in the U-PEO:xCuZnAl composite. These features suggest that the polar integrations between LDH and the host PEO, involving ether-type oxygen atoms, play a significant role in the mobility of the PEO chains. Consequently, the inter-chain interactions of the amorphous polymer phase were significantly affected by the LDH conjugation.

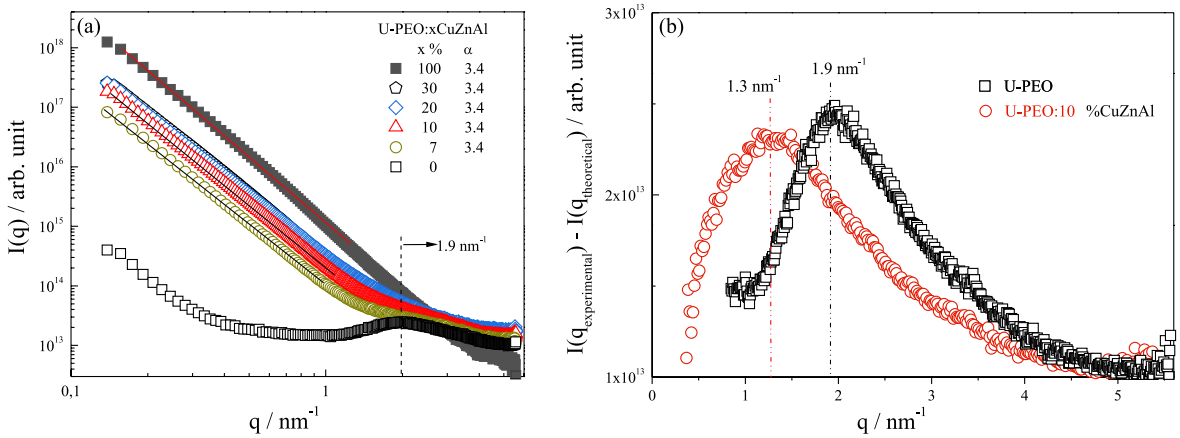

Figure 4. (a) Log-log plots of SAXS curves for U-PEO (x = 0%), and U-PEO:xCuZnAl composites prepared with different percentages of CuZnAl. (b) linear plots of SAXS curves in the region of the U-PEO correlation peak, applying the power law ($I(\mathbf{q})_{Calc} = \mathbf{q}^{-\alpha}$ + constant) subtraction from the experimental ($I(\mathbf{q})_{Exp}$) curve for U-PEO:xLDH (x = 10%).

A significant decrease of the endothermic melting event area was observed after conjugation of the LDH and the U-PEO matrix, reflecting a continuous decrease of the crystallinity degree (D_c) from 23% for the pure U-PEO to 12% for the U-PEO:xLDH conjugation with 30% of CuZnAl. This was consistent with the SAXS data showing a more stretched conformation for the conjugated material and consequent decrease of T_g, resulting from a reduction of the helical PEO conformations of the crystalline polymers. In addition, the DSC profile for U-PEO:LDH showed a broad exothermic peak slightly above the glass transition temperature. This could be explained by a cold crystallization, indicating that the LDH integration hindered the host U-PEO crystallization, due to slower crystallization kinetics, which became sufficiently slow to partially prevent the glass transition during cooling.

Comparison of the FTIR spectra for U-PEO:xLDH, U-PEO, and pure LDH (Figure 6) confirmed the effect of

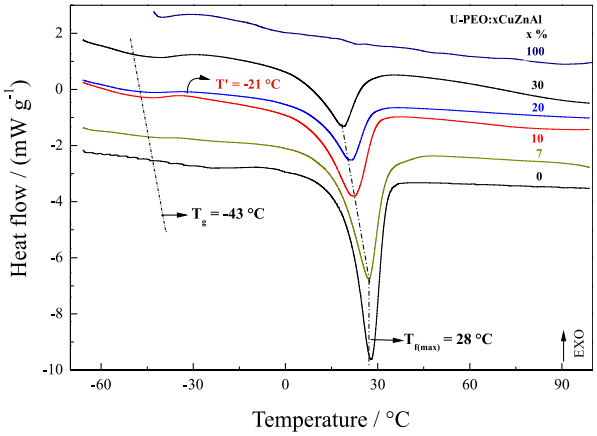

Figure 5. DSC curves for U-PEO:xLDH prepared with different percentages (x) of CuZnAl.

Table 2. Effect of the amount of CuZnAl (x%) in the U-PEO:xLDH composite in the glass transition temperature (T_g), the melting temperature (T_m), the melting enthalpy (ΔH_m) and the percentage of crystalline PEO phase (D_c)

U-PEO:xCuZnAl (x / %)	T_g / ºC	ΔH_m / (J g^{-1})	D_c / %	T_m / ºC
0	–43	44	23	28
7	–43	37	19	27
10	–45	34	17	22
20	–52	28	14	21
30	–52	24	12	19

LDH integration on the PEO inter-chain interactions. The FTIR spectra provided information about the so-called amide vibrations (νC=O$_{carb}$, νN–H), in the range from 1800 to 1500 cm^{-1}, and the C–O$_{eth}$–C backbone stretching mode (νCO$_{eth}$C), in the range from 1200 to 1000 cm^{-1}.[45,65-67] Both regions are known to be sensitive to external perturbations, due to the polymeric conformation changes arising from the specificity and magnitude of hydrogen bonding[68] or interaction with different cations.[66] No significant modification was observed in the amide region within the spectral range from 1700 to 950 cm^{-1} (Figure 6a).

Considering the backbone stretching mode region, from 1200 to 1000 cm^{-1}, the individual components of the broad νCO$_{eth}$C band for the U-PEO hybrid host and the U-PEO:LDH hybrid S-L reactor were obtained from least-square curve profile fitting, as shown in Figures 6b and 6c, respectively. The position (1100 cm^{-1}) of the component located at the higher wavenumber, ascribed to the non-coordinated νCO$_{eth}$C,[67,69] remained invariant after the U-PEO and LDH conjugation. However, the more intense component in the U-PEO spectrum (Figure 6b) showed a

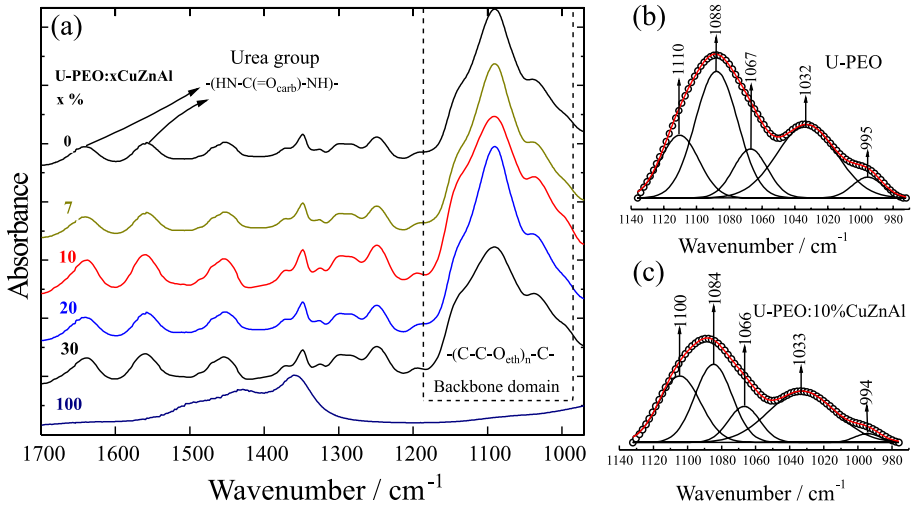

Figure 6. (a) FTIR-ATR spectra in the region from 1700 to 950 cm^{-1} for the U-PEO hybrid host, the U-PEO:xLDH composite prepared with different percentage (x) of CuZnAl. Gaussian fitting of the FTIR spectra in the CO$_{eth}$C backbone region is shown for (b) the U-PEO hybrid host and the (c) OIH:xLDH composite with 10% of CuZnAl.

small downshift, from 1088 to 1084 cm^{-1}, after conjugation and formation of the composite. These features confirmed the interaction between the LDH and the U-PEO host matrix.

Dye removal

Evaluation of the real potential of the new S-L reactor as a catalyst for the degradation of azo dyes using Fenton-like reactions was performed with AB29 selected as a target molecule. The UV-Vis spectra of AB29 were acquired at intervals time of 15 min of the total of 60 min during the Fenton-like reaction using the U-PEO:10%LDH and SC solution and are shown in Figure 7. The initial spectrum (at t = 0 min) showed an absorption band in the visible region (at 602 nm), ascribed to $\pi \rightarrow \pi^*$ transitions of the chromophores, responsible for the blue color of the azo dye, together with a band in the UV region (at 389 nm), ascribed to the azo linkage (–N=N–) and $\pi \rightarrow \pi^*$ transitions of the two adjacent rings of the naphthalene molecule.[70] The temporal evolution of the spectra in Figure 7 indicated the occurrence of the dual process involving absorption and the Fenton-like reaction during the first minutes after contact of the S-L reactor with hydrogen peroxide, leading to continuous and regular decreases of absorbance for both bands. The concentration of AB29, which was adsorbed by the OIH host matrix and degraded by Fenton-like processes, was monitored using the intensity of the blue color at λ = 602 nm, which followed linear behavior, according to equation 6.

The photographs in Figure 7 reveal decolorization of the initial solution and a change in the shade of blue color for the flat cylindrical S-L reactor, after dye absorption/Fenton-like reaction. The original blue color of the S-L

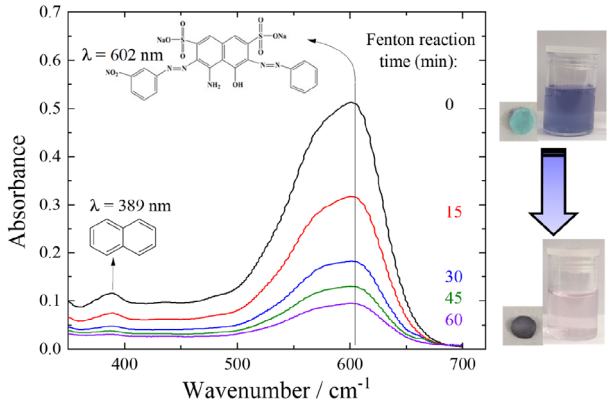

Figure 7. UV-Vis spectra of Acid Blue 29 as a function of contact time with aqueous solution containing 0.1 mg L^{-1} of OIH:10%LDH S-L reactor ([AB29] = 15 mg L^{-1}, [H_2O_2] = 5 mmol L^{-1}). Pictures display the initial (top) and end (down) colors of the cylindrical reactor and the dye solution.

reactor was due to the presence of Cu^{2+} in the CuZnAl LDH conjugated to the U-PEO matrix. The blue shade observed after the catalytic process was due to remaining molecules of undegraded AB29 that had been adsorbed during the dual process. It was reported previously that an OIH hybrid matrix, analogous to the one studied here, had a maximum anionic azo dye absorption capacity that was related to filling of the free volume between adjacent PEO chains.[69]

Elucidation of the LDH:OIH ratio that provided the best AB29 degradation by the Fenton-like process was performed by determining the efficiency of removal of AB29 present in a 15 mg L^{-1} of SC solution, as a function of the amount of LDH integrated into the hybrid host matrix (7, 10, 20, and 30 wt.%) and the dosage of H_2O_2 added to the aqueous solution ([H_2O_2] = 0.002, 0.005, 0.01, 0.05, and 0.09 mol L^{-1}). The results are summarized in Figures 8a

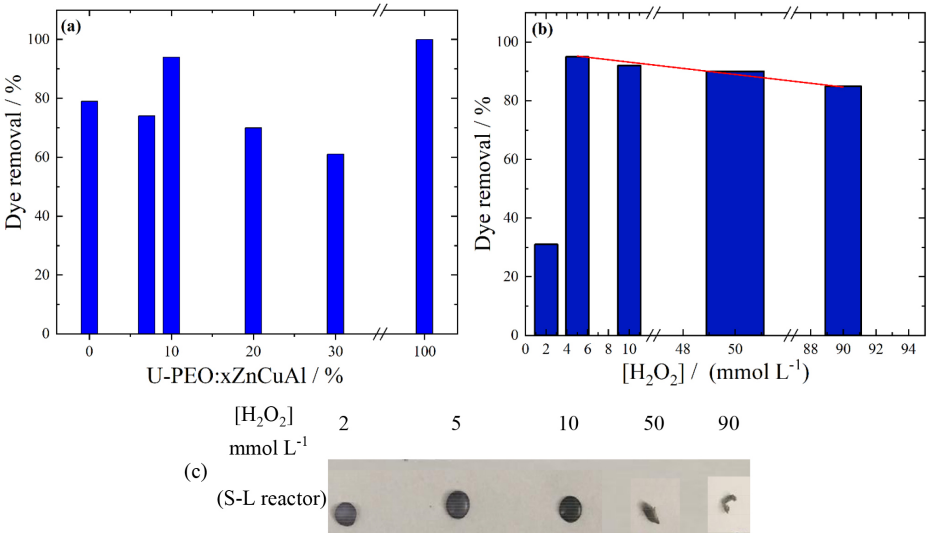

Figure 8. AB29 removal efficiencies after 1 h of Fenton-like reaction from a SC solution (S-L = 0.1 mg L^{-1}, AB29 =15 mg L^{-1} and H_2O_2 = 5 mmol L^{-1}): (a) variation of the U-PEO:xLDH ratio (x = 7, 10, 20, and 30 wt.%), and (b) the hydrogen peroxide concentration (2, 5, 10, 50, and 90 mmol L^{-1}) for U-PEO:10%LDH. (c) Images of the S-L reactors immediately after 1 h of Fenton-like reaction using the hydrogen peroxide concentrations shown in (b).

and 8b. The concentration of AB29 was monitored using the intensity of the blue color, determined at λ = 602 nm.

The effect of the amount of LDH integrated into the U-PEO hybrid matrix was evaluated using solutions containing 15 mg L^{-1} of AB29 and 5 × 10^{-3} mol L^{-1} of H_2O_2. The results, summarized in Figure 8a, showed that the highest removal efficiency (95%) was obtained for the sample containing 10% of LDH catalyst. As expected, below the maximum, the AB29 removal efficiency was directly proportional to the catalyst content, because of the increase of the number of $Cu^{+}\leftrightarrow Cu^{2+}$ redox pair adsorption sites. However, the decreasing dye removal efficiency for LDH content higher than 10% must have been due to decrease of the unoccupied free volume of the host matrix, which limited the diffusion of AB29 to the bulk of the U-PEO hydrogel. This competition for the same free volume space by the LDH catalyst and the AB29 molecules caused a limitation of the azo dye degradation efficiency with increasing amount of the LDH catalyst (see Scheme 1).

In the case of H_2O_2 dosage, it is well known that the classical Fenton process operates with a high molar concentration of H_2O_2 to ensure an acceptable degradation rate.[8] However, it is also known that use of an excessive amount of the oxidant can lead to undesirable parallel reactions,[71] decreasing the reactivity of •OH towards degradation of the target contaminant. Furthermore, hydroxyl radicals (HO•) are highly reactive and attack organic molecules in a non-selective way,[9] so the uncontrolled production of these radicals within the host matrix could be prejudicial to the integrity of the OIH.

The effect of H_2O_2 concentration on the efficiency of dye degradation by the Fenton-like reaction was evaluated by maintaining the concentrations of the S-L reactor catalyst and AB29 constant at 0.1 and 15 mg L^{-1}, respectively. Figure 8b summarizes the results for the dye removal efficiency after 1 h of Fenton-like reaction with different hydrogen peroxide concentrations. The worst efficiency was found for the reaction using 2 mmol L^{-1} of the oxidant, revealing that this H_2O_2 concentration was insufficient to run the degradation reaction quantitatively. In fact, this concentration is lower than the theoretical molar ratio expected for the total mineralization of AB29 from the reaction with H_2O_2.

A maximum decolorization of 95% was obtained for the solution with H_2O_2 at a concentration of 0.005 mol L^{-1}, evidencing the generation of an optimum amount of peroxy-intermediate or hydroxyl radicals[72] required for overall degradation of the dye molecule.[73] A small and continuous decrease to 86% occurred as the H_2O_2 concentration was increased to 0.090 mol L^{-1}, which could have been due to macroscopic damage to the OIH host matrix, as evidenced by the images of the S-L reactors shown in Figure 8c. Given these results, the subsequent reactions were performed using H_2O_2 at a concentration of 5 mmol L^{-1}. Besides resulting in the best dye degradation performance, this peroxide concentration ensured that the integrity of the OIH matrix structure was maintained.

The activity of this new S-L reactor for the decolorization of aqueous solutions of ionic molecules is based on a stepwise mechanism, as follows: (*i*) swelling of OIH due to diffusion of the aqueous solution through the free spaces between PEO chains; (*ii*) sorption of dye molecules on the U-PEO[74] and the LDH catalyst;[75] and (*iii*) degradation of the dye molecules, catalyzed by the LDH. Therefore, to investigate the contribution of each step of this process, the decolorization of the dye solution (AB29 at 15 mg L^{-1}) in the dark was investigated using the different conditions shown in Figure 9: (*i*) AB29 degradation by hydrolysis; (*ii*) Fenton-like degradation by H_2O_2; (*iii*) adsorption by the U-PEO host matrix; (*iv*) adsorption by the U-PEO:CuZnAl S-L reactor; (*v*) adsorption + Fenton-like degradation by the U-PEO:CuZnAl S-L reactor.

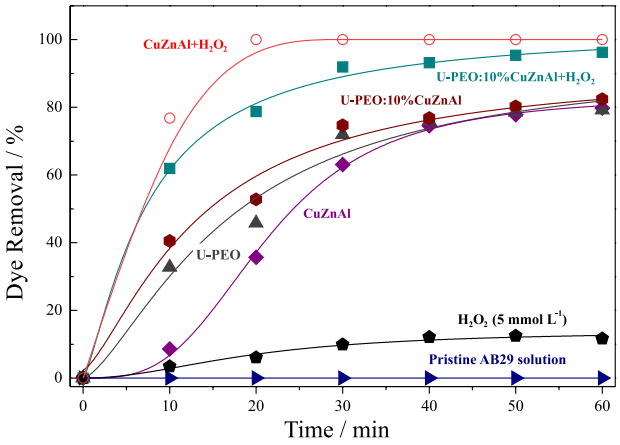

Figure 9. Temporal profiles of AB29 removal from the solutions containing the agents specified on the curves with the following concentrations: [U-PEO:10%CuZnAl] = [[U-PEO] = 0.1 mg L^{-1}, [AB29] = 15 mg L^{-1}, [H_2O_2] = 5 mmol L^{-1}].

Comparison was made of AB29 hydrolysis and dark degradation by H_2O_2 alone. Without any catalyst, but with H_2O_2 at 5 mmol L^{-1}, only 11.7% of the dye was degraded in 1 h. As is known, H_2O_2 photolysis is dependent on UV irradiation, in the UVC region (λ ca. 254 nm), at a wavelength of sufficiently strong energy to generate hydroxyl radicals and run the Fenton-like reactions.[73] Since the data were collected by analysis using the UV spectral range from 700 to 200 nm, this small fraction degraded could be attributed to hydroxyl radicals (HO•) produced by photolysis due to irradiation from the UV instrumentation.

On the other hand, evaluation of dye absorption in the absence of H_2O_2, using 0.3 g of U-PEO, CuZnAl or U-PEO:10%CuZnAl, resulted in very similar removals (79-82%) of AB29 (initial concentration of 15 mg L^{-1}) after 1 h of the experiment. The lower discoloration kinetic by using CuZnAl is an indicative of adsorption of dye molecules between the layers of the lamellar structure.[26,75] However, these classical absorption/adsorption methods mainly result in transfer of the contaminant from wastewater to solid waste.[3] Finally, in the dark experiment using 0.3 g of the S-L reactor and 5 mmol L^{-1} H_2O_2, there was a remarkable increase in the rate of degradation, reaching over 90% degradation in 0.5 h and 96% at the end of the 1 h of Fenton-like reaction. The effectiveness of the Fenton-like degradation could be attributed to the reactions involving hydroxyl radicals ($HO^{\bullet}$) or peroxide radicals ($^{\bullet}O_2H$), according to the mechanisms described previously.[13,76] Moreover, the efficiency of 96% observed for the U-PEO:10%LDH is comparable to the best values reported in Table 1 for different Fenton or Fenton-like catalysts.

Another important experimental factor is the pH susceptibility of Fenton reaction, which usually prefers to occur at low pH,[16] so, the addition of acids in the wastewater may be necessary in operational processes. Herein, the effect of pH on the AB29 removal over the most active U-PEO:10%CuZnAl S-L reactor was investigated, by adjusting the pH with a 2% HNO_3 solution. The time evolution of AB29 discoloration at pH 7, 5 and 3 are summarized in Figure S3 (SI section). It is interesting to note that the discoloration is almost independent of pH, and the AB29 can be degraded almost completely (97.6%) in the pH range between 3 and 7. This may be a consequence of the low sensitivity of CuZnAl to the changes in pH, as indicated by the constancy of ζ-potential in acid solutions (Figure 2). Therefore, the U-PEO:10%CuZnAl S-L reactor can be used without adjusting the pH, which can simplify the pretreatment of wastewater and avoid equipment corrosion.

The potential for reuse is one of the greatest advantages of a heterogeneous catalyst, with its use in successive cycles also providing useful information about catalytic stability. Different LDH catalysts have shown good recyclability when reused in the degradation of various azo dyes using the Fenton-like reaction.[77] Therefore, the evaluation was made of the recyclability of the U-PEO:10CuZnAl material.

The catalyst showed a regular reduction in activity after every run. As shown in Figure 10a, 96% degradation of AB29 by the S-L reactor was obtained in the first cycle, followed by a modest decrease to 88% in the second cycle, which was still higher than in the first cycle using only absorption by U-PEO and U-PEO:CuZnAl (ca. 79%, Figure 10b). In the fourth cycle, the decolorization decreased to 65%. Nevertheless, this recycled S-L reactor presented better performance than obtained with powdered LDH catalyst, such as in the case of a CuZnAl LDH powder that showed around 40% efficiency in the Fenton-like degradation of methyl orange (20 mg L^{-1}).[78] The decreasing efficiency could be explained by the progressive accumulation of undegraded AB29 molecules adsorbed on the OIH matrix, which reduced the kinetics of the adsorption process. However, a more in deep study of the structural evolution of U-PEO:10%CuZnAl S-L during reuse cycle must be done to maximize the life time of this new S-L reactor.

Conclusions

The experimental results demonstrated the efficacy of the new S-L reactor as a catalyst for azo dye degradation

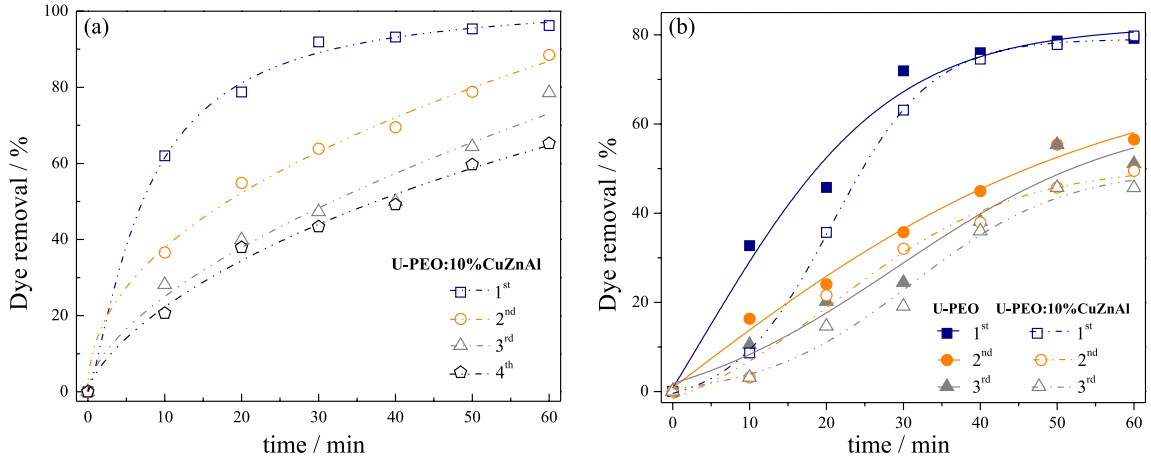

Figure 10. Reusability of (a) U-PEO:10%CuZnAl applied in Fenton-like degradation of AB29 under the standard conditions, and (b) U-PEO and U-PEO:10%CuZnAl applied in AB29 adsorption under the standard conditions, without H_2O_2.

by Fenton-like reactions, using AB29 as a model molecule. The integration of LDH into the U-PEO matrix, as evidenced by scanning electron microscopy, X-ray diffraction and small-angle X-ray scattering analyses, indicated the preservation of the LDH lamellar structure within the composite material. SAXS analysis revealed a downshift of the siloxane nodes correlation peak position, evidencing LDH occupation within the free volume of the U-PEO matrix and reorganization of the PEO chain conformation. Hence, the U-PEO:LDH conjugation not only preserved the LDH structure, but also influenced the conformation of the polyether chains.

The conjugation of LDH within the U-PEO matrix led to subtle but discernible alterations of its thermal and structural properties. The glass transition (T_g) and the melting (T_m) temperatures decreased continuously with the percentage (x%) of LDH in the composite, indicating the increase of the PEO chain mobility. Moreover, a reduction in the degree of crystallinity of U-PEO was observed after conjugation with LDH. This reduction reflected a transition from helical to stretched conformations in the polymer, due to the dispersion of LDH into the free volume of the PEO chains. The FTIR spectra showed minimal alterations in the amide and backbone stretching regions, indicating weak interactions between LDH and U-PEO.

The mechanism of dye removal using the S-L reactor involved multiple steps: swelling of the matrix, due to water diffusion; sorption of the dye onto U-PEO and LDH; and subsequent degradation catalyzed by LDH. The degradation was monitored by UV-Vis spectroscopy, revealing a steady decrease in absorbance and signaling the degradation of AB29 within minutes. The results indicated an optimal LDH content of 10% for maximum removal efficiency by enhancing the $Cu^{+}\leftrightarrow Cu^{2+}$ redox pair active sites. A hydrogen peroxide concentration of 5 mmol L^{-1} was found to be optimal, ensuring both efficient degradation and minimal hydroxyl radical production, preserving the integrity of the OIH matrix.

Evaluation of the recyclability of the catalyst showed a gradual reduction in activity over successive cycles, although the performance remained superior to that of the pure powdered LDH catalyst. This reduction was attributed to undegraded AB29 molecules saturating the OIH matrix, which hindered the adsorption of dye molecules, consequently decreasing the dye removal efficiency in subsequent cycles.

Overall, the findings provide valuable insights into optimizing the LDH content and the hydrogen peroxide concentration for efficient azo dye degradation. The developed S-L reactor has excellent potential as a heterogeneous catalyst for effective dye removal.

Supplementary Information

Supplementary data (Figure S1: nitrogen adsorption-desorption isotherms for the CuZnAl powder; Figure S2: Log-log plot of experimental SAXS curve (black) in the **q** region of correlation peak and the theoretical curve (red) calculated by the power law and background scattering ($I(\mathbf{q})_{Calc} = \mathbf{q}^{-\alpha} + cte$); Figure S3: temporal profiles of AB29 degradation by U-PEO:10%CuZnAl in solutions at different pH) are available free of charge at http://jbcs.sbq.org.br as PDF file.

Acknowledgments

This study was financed in part by Coordenação de Aperfeiçoamento de Pessoal de Nível Superior - Brasil (CAPES, Finance Code 001, process nº. 88887.357796/2019-00) and CNPq (grants 142495/2013-1, 203031/2015-6, 168263/2017-0, 304592/2019-6, and 401679/2013-6). This work is a collaborative research project of the members of the National Institute on Advanced Eco-Efficient Cement-Based Technologies (FAPESP INCT 2014 50948-3; 465593/2014-3). The authors thank Dr Marina Magnani and Dr Marina Paiva Abuçafy for the SEM measurements, and the Brazilian National Synchrotron Light Laboratory for measurements performed at the SAXS1 beamline.

Author Contributions

Gustavo Palácio was responsible for data curation, formal analysis, investigation, methodology, writing original draft; Camila T. Piza for data curation, formal analysis, investigation, methodology, writing original draft; Maria Luiza Batista for data curation, investigation, methodology, writing original draft; Caio C. dos Santos for data curation, formal analysis; Sandra Helena Pulcinelli for conceptualization, formal analysis, funding acquisition, investigation, methodology, resources, writing original draft; Celso V. Santilli for conceptualization, formal analysis, funding acquisition, investigation, methodology, supervision, validation, writing original draft.

References

1. Amin, M. T.; Alazba, A. A.; Manzoor, U.; *Adv. Mater. Sci Eng.* **2014**, ID 825910. [Crossref]
2. Rodriguez-Narvaez, O. M.; Peralta-Hernandez, J. M.; Goonetilleke, A.; Bandala, E. R.; *Chem. Eng. J.* **2017**, *323*, 361. [Crossref]
3. Neamtu, M.; Yediler, A.; Siminiceanu, I.; Kettrup, A.; *J. Photochem. Photobiol., A* **2003**, *161*, 87. [Crossref]

4. Miklos, D. B.; Remy, C.; Jekel, M.; Linden, K. G.; Drewes, J. E.; Hübner, U.; *Water Res.* **2018**, *139*, 118. [Crossref]
5. Kurian, M.; *Cleaner Eng. Technol.* **2021**, *2*, 100090. [Crossref]
6. Soon, A. N.; Hameed, B. H.; *Appl. Catal., A* **2013**, *450*, 96. [Crossref]
7. Pignatello, J. J.; Oliveros, E.; MacKay, A.; *Crit. Rev. Environ. Sci. Technol.* **2006**, *36*, 1. [Crossref]
8. Dhakshinamoorthy, A.; Navalon, S.; Alvaro, M.; Garcia, H.; *ChemSusChem* **2012**, *5*, 46. [Crossref]
9. Vilhunen, S.; Sillanpää, M.; *Rev. Environ. Sci. Biotechnol.* **2010**, *9*, 323. [Crossref]
10. Gawande, M. B.; Goswami, A.; Felpin, F. X.; Asefa, T.; Huang, X.; Silva, R.; Zou, X.; Zboril, R.; Varma, R. S.; *Chem. Ver.* **2016**, *116*, 3722. [Crossref]
11. Watts, R. J.; Sarasa, J.; Loge, F. J.; Teel, A. L.; *J. Environ. Eng.* **2005**, *131*, 158. [Crossref]
12. Fu, Y.; Fu, X.; Song, W.; Li, Y.; Li, X.; Yan, L.; *Materials* **2023**, *16*, 5723. [Crossref]
13. Chen, T.; Zhu, Z.; Zhang, H.; Shen, X.; Qiu, Y.; Yin, D.; *ACS Omega* **2019**, *4*, 1982. [Crossref]
14. Fenton, H. J. H.; *J. Chem. Soc. Trans.* **1894**, *65*, 899. [Crossref]
15. Taylor, W.; Weiss, J.; *J. Chem. Phys.* **1953**, *21*, 1419. [Crossref]
16. Bokare, A. D.; Choi, W.; *J. Hazard. Mater.* **2014**, *275*, 121. [Crossref]
17. Nieto-Juarez, J. I.; Pierzchla, K.; Sienkiewicz, A.; Kohn, T.; *Environ. Sci. Technol.* **2010**, *44*, 3351. [Crossref]
18. Kim, J. K.; Metcalfe, I. S.; *Chemosphere* **2007**, *69*, 689. [Crossref]
19. Bradu, C.; Frunza, L.; Mihalche, N.; Avramescu, S. M.; Neaţă, M.; Udrea, I.; *Appl. Catal., B* **2010**, *96*, 548. [Crossref]
20. Salem, I. A.; *Appl. Catal., B* **2000**, *28*, 153. [Crossref]
21. Fink, L.; Dror, I.; Berkowitz, B.; *Chemosphere* **2012**, *86*, 144. [Crossref]
22. Baldrian, P.; Zervakis, G. I.; Merhautová, V.; Ntougias, S.; Ehaliotis, C.; Nerud, F.; *Folia Microbiol.* **2006**, *51*, 337. [Crossref]
23. Verma, P.; Shah, V.; Baldrian, P.; Gabriel, J.; Stopka, P.; Trnka, T.; Nerud, F.; *Chemosphere* **2004**, *54*, 291. [Crossref]
24. Bali, U.; Karagözoğlu, B.; *Dyes Pigm.* **2007**, *74*, 73. [Crossref]
25. Zhan, Y.; Zhou, X.; Fu, B.; Chen, Y.; *J. Hazard. Mater.* **2011**, *187*, 348. [Crossref]
26. Gonçalves, R. G. L.; Mendes, H. M.; Bastos, S. L.; D'Agostino, L. C.; Tronto, J.; Pulcinelli, S. H.; Santilli, C. V.; Leal Neto, J.; *Appl. Clay. Sci.* **2020**, *187*, 105477. [Crossref]
27. Fan, G.; Li, F.; Evans, D. G.; Duan, X.; *Chem. Soc. Rev.* **2014**, *43*, 7040. [Crossref]
28. Mishra, G.; Dash, B.; Pandey, S.; *Appl. Clay Sci.* **2018**, *153*, 172. [Crossref]
29. Daud, M.; Hai, A.; Banat, F.; Wazir, M. B.; Habib, M.; Bharath, G.; Al-Harthi, M. A.; *J. Mol. Liq.* **2019**, *288*, 110989. [Crossref]
30. Chaillot, D.; Bennici, S.; Brendlé, J.; *Environ. Sci. Pollut. Res.* **2021**, *28*, 24375. [Crossref]
31. Takács, D.; Varga, G.; Csapó, E.; Jamnik, A.; Tomšič, M.; Szilágyi, I.; *J. Phys. Chem. Lett.* **2022**, *13*, 11850. [Crossref]
32. Ballottin, D.; Fulaz, S.; Cabrini, F.; Tsukamoto, J.; Durán, N.; Alves, O. L.; Tasic, L.; *Mater. Sci. Eng., C* **2017**, *75*, 582. [Crossref]
33. Gimenez, F. I.; Ferreira, O. P.; Alves, O. L.; *BR pat. 0200354-6*, 2002.
34. Ferreira, O. P.; Alves, O. L.; Gouveia, D. X.; Souza Filho, A. G.; De Paiva, J. A. C.; Filho, J. M.; *J. Solid State Chem.* **2004**, *177*, 3058. [Crossref]
35. Ferreira, O. P.; de Moraes, S. G.; Durán, N.; Cornejo, L.; Alves, O. L.; *Chemosphere* **2006**, *62*, 80. [Crossref]
36. Pelalak, R.; Hassani, A.; Heidari, Z.; Zhou, M.; *Chem. Eng. J.* **2023**, *474*, 145511. [Crossref]
37. Wang, H.; Zhang, Z.; Jing, M.; Tang, S.; Wu, Y.; Liu, W.; *Appl. Clay. Sci.* **2020**, *186*, 105433. [Crossref]
38. Peng, X.; Wang, M.; Hu, F.; Qiu, F.; Zhang, T.; Dai, H.; Cao, Z.; *J. Environ. Manage.* **2018**, *220*, 173. [Crossref]
39. Wu, Z.; Gu, Y.; Xin, S.; Lu, L.; Huang, Z.; Li, M.; Cui, Y.; Fu, R.; Wang, S.; *Chem. Eng. J.* **2022**, *434*, 134574. [Crossref]
40. Costa-Serge, N. M.; Gonçalves, R. G. L.; Rojas-Mantilla, H. D.; Santilli, C. V.; Hammer, P.; Nogueira, R. F. P.; *J. Hazard. Mater.* **2021**, *413*, 125388. [Crossref]
41. Dou, L.; Zhang, H.; *J Mater. Chem. A* **2016**, *4*, 18990. [Crossref]
42. Dahmouche, K.; Santilli, V.; Pulcinelli, S. H.; Craievich, A. F.; *J. Phys. Chem. B* **1999**, *103*, 4937. [Crossref]
43. Croissant, J. G.; Cattoën, X.; Durand, J.-O.; Chi Man, M. W.; Khashab, N. M.; *Nanoscale* **2016**, *8*, 19945. [Crossref]
44. Zaldivar, M. P.; Santilli, C. V.; Covas, C. A. P.; Pulcinelli, S. H.; *J. Therm. Anal. Calorim.* **2017**, *130*, 791. [Crossref]
45. Palácio, G.; Pulcinelli, S. H.; Mahiou, R.; Boyer, D.; Chadeyron, G.; Santilli, C. V.; *ACS Appl. Mater. Interfaces* **2018**, *10*, 37364. [Crossref]
46. Strawhecker, K. E.; Manias, E.; *Chem. Mater.* **2003**, *15*, 844. [Crossref]
47. Molina, E. F.; Nogueira, C. R.; Chiavacci, L. A.; Pulcinelli, S. H.; Briois, V.; Santilli, C. V.; *J. Solgel Sci. Techonol.* **2014**, *70*, 317. [Crossref]
48. Jesus, C. R. N.; Molina, E. F.; Pulcinelli, S. H.; Santilli, C. V.; *ACS Appl. Mater. Interfaces* **2018**, *10*, 19059. [Crossref]
49. de Santana, W. M. O. S.; Abramson, S.; Fini, R.; Caetano, B. L.; Ménager, C.; Pulcinelli, S. H.; Santilli, C. V.; *ACS Appl. Polym. Mater.* **2021**, *3*, 4837. [Crossref]
50. Cavani, F.; Trifirò, F.; Vaccari, A.; *Catal. Today* **1991**, *11*, 173. [Crossref]
51. Santilli, C. V.; Chiavacci, L. A.; Lopes, L.; Pulcinelli, S. H.; Oliveira, A. G.; *Chem. Mater.* **2009**, *21*, 463. [Crossref]
52. Gonçalves. C. M.; Bermudez, V. D. Z.; Sa, R. A.; Carlos, L. D.; Ostroviskii, D.; Rocha, J.; *Chem. Mater.* **2004**, *16*, 2530. [Crossref]

53. Mori, T.; Akamatsu, M.; Okamoto, K.; Sumita, M.; Tateyama, Y.; Sakai, H.; Hill, J. P.; Abe, M.; Ariga, K.; *Sci. Technol. Adv. Mater.* **2013**, *14*, 15002. [Crossref]
54. Gregg, S. J.; Sing, K. S. W.; *Adsorption, Surface Area and Porosity*, 2nd ed.; Academic Press: London, UK, 1997.
55. Salem, I. A.; El-ghamry, H. A.; El-ghobashy, M. A.; *J. Basic Appl. Sci.* **2014**, *3*, 186. [Crossref]
56. Han, J.; Zeng, H.; Xu, S.; Chen, C.; Liu, X.; *Appl. Catal., A* **2016**, *527*, 72. [Crossref]
57. Santos, R. M. M.; Briois, V.; Martins, L.; Santilli, C. V.; *ACS. Appl. Mater. Interfaces* **2021**, *13*, 26001. [Crossref]
58. Joy, M.; Iyengar, S. J.; Chakraborty, J.; Ghosh, S.; *Front. Mater. Sci.* **2017**, *11*, 395. [Crossref]
59. Xu, Z. P.; Jin, Y.; Liu, S.; Hao, Z. P.; Lu, G. Q.; *J. Colloid Interface Sci.* **2008**, *326*, 522. [Crossref]
60. Truffault, L.; Rodrigues, F. D.; Salgado, H. R. N.; Santilli, C. V.; Pulcinelli, S. H.; *Colloids Surf., B* **2016**, *147*, 151. [Crossref]
61. Santos, R. M. M.; Tronto, J.; Briois, V.; Santilli, C. V.; *J. Mater. Chem. A* **2017**, *5*, 9998. [Crossref]
62. Schnablegger, H.; Singh, Y.; *The SAXS Guide, Getting Acquainted with the Principles*, 5th ed.; Anton Paar GmbH: Graz, Austria, 2013.
63. Gonçalves, M. C.; Fernandes, I. C.; Hümmer, J.; Bermudez, V. D. Z.; *Vib. Spectrosc.* **2011**, *57*, 187. [Crossref]
64. Wang, J.; Zhang, H.; Zheng, H.; Xuan, X.; *Chem. Phys.* **2006**, *325*, 538. [Crossref]
65. Palácio, G.; Boyer, D.; Therias, S.; Pulcinelli, S. H.; Mahiou, R.; Chadeyron, G.; Santilli, C. V.; *Polymer* **2019**, *177*, 102. [Crossref]
66. Nunes, S. C.; de Zea Bermudez, V.; Cybinska, J.; Ferreira, R. A. S.; Legendziewicz, J.; Carlos, L. D.; Silva, M. M.; Smith, M. J.; Ostrovskii, D.; Rocha, J.; *J. Mater. Chem.* **2005**, *15*, 3876. [Crossref]
67. De Zea Bermudez, V.; Carlos, L. D.; Alcácer, L.; *Chem. Mater.* **1999**, *11*, 569. [Crossref]
68. Nunes, S. C.; Bermudez, V. D. Z.; Ostrovskii, D.; Barbosa, P. C.; Silva, M. M.; Smith, M. J.; *Chem. Phys.* **2008**, *345*, 32. [Crossref]
69. Molina, E. F.; Parreira, R. L. T.; De Faria, E. H.; de Carvalho, H. W. P.; Caramori, G. F.; Coimbra, D. F.; Nassar, E. J.; Ciuffi, K. J.; *Langmuir* **2014**, *30*, 3857. [Crossref]
70 Sahoo, M. K.; Sayoo, L.; *Desalin. Water Treat.* **2014**, *52*, 3411. [Crossref]
71. Costa, N. M.; Silva, V. M.; Damaceno, G.; Sousa, R. M. F.; Richter, E. M.; Machado, A. E. H.; Trov, A. G.; *J. Environ. Manage.* **2017**, *203*, 229. [Crossref]
72. Wang, H.; Jing, M.; Wu, Y.; Chen, W.; Ran, Y.; *J. Hazard. Mater.* **2018**, *353*, 53. [Crossref]
73. Ghaly, M. Y.; Härtel, G.; Mayer, R.; Haseneder, R.; *Waste Manage.* **2001**, *21*, 41. [Crossref]
74. Bermúdez, Y. H.; Truffault, L.; Pulcinelli, S. H.; Santilli, C. V.; *Appl. Clay Sci.* **2018**, *152*, 158. [Crossref]
75. dos Santos, R. M. M.; Gonçalves, R. G. L.; Constantino, V. R. L.; Santilli, C. V.; Borges, P. D.; Tronto, J.; Pinto, F. G.; *Appl Clay Sci.* **2017**, *140*, 132. [Crossref]
76. Zhang, H.; Li, G.; Deng, L.; Zeng, H.; Shi, Z.; *J. Colloid Interface Sci.* **2019**, *543*, 183. [Crossref]
77. Guo, X. X.; Hu, T. T.; Meng, B.; Sun, Y.; Han, Y. F.; *Appl. Catal., B* **2020**, *260*, 118157. [Crossref]
78. Li, J.; Zhang, S.; Chen, Y.; Liu, T.; Liu, C.; Zhang, X.; Yi, M.; Chu, Z.; Han, X.; *RSC Adv.* **2017**, *7*, 29051. [Crossref]

Submitted: January 25, 2024
Published online: June 4, 2024